Delft University of Technology

Multi-Carrier Energy Home Energy Management System Using Genetic Algorithms and Random Forest Predictions

Alpizar Castillo, J.J.; Fu, Aihui; Ramirez Elizondo, L.M.; Cvetkovic, Milos; Bauer, Pavol

Important note
To cite this publication, please use the final published version (if applicable).
Please check the document version above.

Multi-Carrier Energy Home Energy Management System Using Genetic Algorithms and Random Forest Predictions

Joel Alpízar-Castillo
Delft University of Technology
Delft, The Netherlands
J.J.AlpizarCastillo@tudelft.nl

Aihui Fu
Delft University of Technology
Delft, The Netherlands
A.Fu@tudelft.nl

Laura Ramírez-Elizondo
Delft University of Technology
Delft, The Netherlands
L.M.RamirezElizondo@tudelft.nl

Milos Cvetkovic
Delft University of Technology
Delft, The Netherlands
M.Cvetkovic@tudelft.nl

Pavol Bauer
Delft University of Technology
Delft, The Netherlands
P.Bauer@tudelft.nl

Abstract—The energy transition encourages using heat pumps at the residential level, which results in a multi-carrier energy system when combined with PV and battery storage. Optimally controlling such systems has proven challenging. The numerous constraints required, different response times per energy carrier, and the need for forecasting methods also increase the complexity and computational cost. We propose an adaptable energy management system strategy for any system architecture with a reduced number of constraints using genetic algorithms with a discrete-continuous approach for the power setpoints. Using random forest regression, we also created short-term estimation models for the PV generation and electric and thermal demand, with error distributions centred near 0 %. Our results demonstrate that the strategy can solve the power allocation problem in the order of 1 s, including forecasting 60 minutes, minimizing electric costs, and ensuring thermal comfort.

Index Terms—Energy Management System, Energy Storage, Genetic Algorithm, Multi-Carrier Energy systems, Random Forest

I. INTRODUCTION

The inclusion of distributed renewable energy sources and electric vehicles in the energy mix has accelerated the energy transition in the last decade. More recently, heating electrification has gained momentum, albeit still heavily dependent on fossil fuels. Therefore, current research proposes the creation of multi-carrier energy systems (MCES) to combine heat and electrical generation, consumption and storage [1]. Recent studies have demonstrated that such combinations help minimize the impact of distributed renewable energy systems (DRES) in the distribution networks if an adequate control strategy is implemented [2]. However, controlling such complex systems has proven challenging for energy management

system (EMS) designers, as their combined models are generally non-linear, non-convex, and heavily constrained, resulting in high computation costs and convergence difficulties [3].

Different energy management system strategies have been proposed in the literature in an attempt to overcome those challenges. Rule-based controls, also known as heuristics, have been commonly used in implementations despite requiring numerous correlations and operation cases since they usually do not show convergence challenges [4]. Nevertheless, they cannot guarantee optimality and rarely use predictions. Thus, more complex optimization strategies have been proposed to handle uncertainty, consider multiple objectives simultaneously, or ensure optimality. For instance, [5] proposed a real-time home energy management system controller using mixed-integer linear programming for a multi-objective problem, achieving cost minimization. An optimization for controlling a multi-carrier system for demand response applications was solved using mixed-integer linear programming by [6] to minimize the operative costs, highlighting the importance of energy storage to provide flexibility to the grid. Day-ahead and real-time participation of an aggregated MCES were studied in [7], using an event-triggered-based distributed algorithm, but the internal energy flow control between the assets was not considered. In [8], the EMS minimized the ageing of the battery energy storage system (BESS) and total energy cost in a residential MCES, reducing the grid costs up to 45 % when compared with controllers that do not consider the degradation of the batteries. A distributed energy management system using sub-gradient averaging consensus was proposed in [9] for real-time control of coupled energy hubs, achieving optimality despite challenges in the convergence rate.

A review in [10] evaluated different artificial intelligence techniques used for power allocation optimization and parameter prediction, concluding that more research is still required to couple such applications given their complexity and compu-

tational cost. The work in [11] used the non-dominated sorting genetic algorithm II to control in real-time the power flow of a multi-carrier energy system in Italy comprised of a renewable energy source system, an EV charger, a water electrolyzer and a fuel cell. The objective functions included the total energy cost and the deviation of a setpoint the distribution system operator (DSO) requested to assist in grid balancing. Dynamic fuzzy logic was used by [12] to optimize renewable energy utilization and minimize electric and gas purchases from the grid, achieving a reduction of up to 80 % in the electric grid. A comparison of gate recurrent unit temporal convolutional network and deep Q-network was done by [13] as energy management strategies for a multi-carrier system, resulting in an economical cost reduction of 14.5 % when using the former.

The literature agrees that computational cost is one of the main challenges to implementing successful energy management systems, especially for multi-carrier energy systems. In addition, [14] reviewed the available simulation and optimization tools, highlighting that coupling the different carriers remains challenging and that many available tools require a license, urging for modular, open-source alternatives. For this reason, an accessible EMS strategy that balances the computational cost and the accuracy is required. Thus, the contributions of this paper are:

- proposing a modular genetic algorithm (GA) EMS strategy for short-term control of the power flow between the assets of a household multi-carrier energy system, intrinsically adaptable to different system architectures, forecasting methods and time horizons,
- implementing a random forest forecast to estimate the load profile, temperature and irradiance for the controller prediction horizon, and
- evaluating the performance of the proposed algorithm considering thermal comfort, energy cost, equivalent CO_2 emissions and computational cost for typical winter and summer conditions in The Netherlands, and different prediction horizons.

The code used for this paper was developed in Python and is available in [15].

II. MULTI-CARRIER ENERGY SYSTEM

For this work, we considered a PV system, a BESS, a heat pump (HP), a thermal energy storage system (TESS) and a solar collector coupled in a multi-carrier energy system. For real-time control, measurements are used for the PV and solar collectors; therefore, they do not require a model. The governing equations for the remaining components are summarized as follows.

A. Battery Energy Storage System

We modelled the energy available in the battery energy storage system as

$$E_{\text{BESS}}(k+1) = E_{\text{BESS}}(k) + \Delta E_{\text{BESS}}(k) - E^{\text{SD}}(k), \quad (1)$$

where $E_{\text{BESS}}(k)$ is the current state of the battery, $E^{\text{SD}}(k)$ is the energy lost due to self-discharge during the previous timestep Δt, and

$$\Delta E_{\text{BESS}}(k) = \begin{cases} \eta^c_{\text{BESS}}(k) P_{\text{BESS}}(k) \Delta t & \forall P_{\text{BESS}}(k) < 0 \\[2ex] \dfrac{P_{\text{BESS}}(k)}{\eta^d_{\text{BESS}}(k)} \Delta t & \forall P_{\text{BESS}}(k) > 0 \end{cases} \quad (2)$$

is the change in energy due to the power delivered or absorbed by the battery during discharge and charge, with efficiencies η^d_{BESS} and η^c_{BESS} respectively [16].

B. Heat Pump

Using the model proposed in [17], we were able to simulate an air-to-water heat pump coefficient of performance (COP) as

$$\text{COP}(k) = 7.90471 e^{-0.024[T_{\text{ret}}(k) - T_{\text{amb}}(k)]}, \quad (3)$$

where T_{ret} is the temperature of the water in the inlet of the heat pump, and T_{amb} is the ambient temperature. The thermal power of the heat pump is then calculated as

$$\dot{Q}_{\text{HP}}(k) = \eta_{\text{HP}} \dot{m}_f c_f \left[T_{\text{sup}} - T_{\text{ret}}(k) \right] = \text{COP}(k) P_{\text{HP}}(k), \quad (4)$$

where η_{HP} is the heat exchanger efficiency, $\dot{m}_f$ is the mass flow in the thermal network, c_f is the fluid specific heat capacity, T_{sup} is the desired supply temperature and P_{HP} is the electrical power consumed by the heat pump.

C. Thermal Energy Storage System

We assumed a closed, well-mixed water tank as the thermal energy storage system, i.e., we did not consider any mass exchange between the TESS and its surroundings or the house [18]. In this case, the tank has separated charge and discharge heat exchangers; therefore, it can perform both simultaneously. Its energy is given by

$$Q_{\text{TESS}}(k+1) = Q_{\text{TESS}}(k) + \left[\dot{Q}^{in}_{\text{TESS}}(k) - \dot{Q}^{out}_{\text{TESS}}(k) \right] \Delta t, \quad (5)$$

with

$$\dot{Q}^{in}_{\text{TESS}}(k) = \eta^c_{\text{TESS}}(k) \left[\dot{Q}^{\text{TESS}}_{\text{SC}}(k) + \dot{Q}^{\text{TESS}}_{\text{HP}}(k) \right] \quad (6)$$

and

$$\dot{Q}^{out}_{\text{TESS}}(k) = \frac{\dot{Q}_{\text{TESS}}(k)}{\eta^d_{\text{TESS}}(k)} + \dot{Q}^{\text{SD}}(k), \quad (7)$$

where $\dot{Q}^{in}_{\text{TESS}}$ and $\dot{Q}^{out}_{\text{TESS}}$ are the charge and discharge thermal powers, respectively, η^c_{TESS} and η^d_{TESS} are the charge and discharge efficiencies, respectively, $\dot{Q}^{\text{TESS}}_{\text{SC}}$ and $\dot{Q}^{\text{TESS}}_{\text{HP}}$ are the thermal powers from the solar collector and the heat pump used to charge the TESS, and $\dot{Q}^{\text{SD}}$ is the self-discharge thermal power. For this paper, we considered that the TESS would be placed underground; thus, the self-discharge is mainly given by the temperature difference between the fluid temperature and the soil around it, resulting in

$$\dot{Q}^{\text{SD}}(k) = \dot{Q}^{\text{SD}}_{\text{top}}(k) + \dot{Q}^{\text{SD}}_{\text{sides}}(k) + \dot{Q}^{\text{SD}}_{\text{bottom}}(k) \quad (8)$$

with

$$\dot{Q}^{\text{SD}}_{\text{top}}(k) = U_{\text{TESS}} A_{\text{top}} \left[T_{\text{TESS}}(k) - T_{\text{s}}(y = y_0, k) \right], \quad (9)$$

1038

$$\dot{Q}_{\text{sides}}^{\text{SD}}(k) = \sum_{i=1}^{n} U_{\text{TESS}} A_{\Delta y} \left[T_{\text{TESS}}(k) - T_{\text{s}}(y_i, k) \right], \qquad (10)$$

and

$$\dot{Q}_{\text{bottom}}^{\text{SD}}(k) = U_{\text{TESS}} A_{\text{bottom}} \left[T_{\text{TESS}}(k) - T_{\text{s}}(y = y_f, k) \right], \quad (11)$$

where $\dot{Q}_{\text{top}}^{\text{SD}}$, $\dot{Q}_{\text{sides}}^{\text{SD}}$ and $\dot{Q}_{\text{bottom}}^{\text{SD}}$ are the self-discharge associated with the temperature difference between the fluid and the soil temperature at the top (depth $y = y_0$), walls and bottom of the tank (depth $y = y_f$) [18].

Similar to (5), the temperature of the fluid in the tank is given by

$$T_{\text{TESS}}(k+1) = T_{\text{TESS}}(k) + \frac{\Delta t \left[\dot{Q}_{\text{TESS}}^{\text{in}}(k) - \dot{Q}_{\text{TESS}}^{\text{out}}(k) \right]}{mc}, \quad (12)$$

where m and c are the fluid mass and specific heat. Finally, the state-of-charge of the TESS can be expressed as a function of its temperature as

$$SoC_{\text{TESS}} = \frac{\Delta T(k)}{\Delta T^{\max}} = \frac{T(k) - T^{\min}}{T^{\max} - T^{\min}}. \qquad (13)$$

D. Electric Demand

For this work, we used the probabilities indicated by [19] for using common household appliances, following the probability function

$$P_L(k) = \sum_{i=1}^{n} P_i(k) \, \mathbb{P}_i \left(\{ \omega_i(k) \in \Omega_i(k) \} \right) \qquad (14)$$

as proposed in [18], where P_i is the appliance power, $\mathbb{P}_i$ is the probability of that appliance to be used at the event space Ω_i are at the instant k.

E. Thermal Demand

We considered only space heating as a thermal demand and neglected the heat transfer between rooms to the ground and the radiative heat transfer. Following the work in [18], the total thermal power needed for space heating is given by

$$\dot{Q}_D = \dot{Q}_L + \dot{Q}_v + \dot{Q}_i \qquad (15)$$

as a function of the thermal power loss through walls, windows and roof due to the thermal difference between indoor and outdoor temperatures, T_{in} and T_{out} respectively,

$$\dot{Q}_L(k) = \sum_{i=1}^{n} U_i A_i \left[T_{\text{in}}(k) - T_{\text{out}}(k) \right], \qquad (16)$$

the ventilation losses

$$\dot{Q}_v(k) = c_a \rho_a q_v \left[T_{\text{in}}(k) - T_{\text{out}}(k) \right], \qquad (17)$$

and infiltration losses

$$\dot{Q}_i(k) = c_a \rho_a q_i \left[T_{\text{in}}(k) - T_{\text{out}}(k) \right], \qquad (18)$$

where the ventilation and infiltration airflow, q_i and q_v, can be estimated following the method suggested by the ASHRAE [20] and c_a and ρ_a are the specific heat capacity and density of the air.

Based on the thermal load presented in (15), one can estimate the indoor temperature with

$$T_{\text{in}}(k+1) = T_{in}(k) + \frac{\Delta t \sum_{i=1}^{n} \dot{Q}_i}{\sum_{i=1}^{n} m_i c_i} \qquad (19)$$

as a function of the net thermal power exchange between the solar collector $\dot{Q}_{\text{SC}}$, thermal energy storage system $\dot{Q}_{\text{TESS}}$, heat pump $\dot{Q}_{\text{HP}}$ and total thermal demand $\dot{Q}_D$

$$\sum_{i=1}^{n} \dot{Q}_i = \dot{Q}_{\text{SC}}(k) + \dot{Q}_{\text{TESS}}(k) + \dot{Q}_{\text{HP}}(k) - \dot{Q}_D(k). \qquad (20)$$

F. Coupled system

The elements previously described are coupled through the household's electric and thermal networks. The former consists of an electric connection in the main electric box of the house, respecting the electric power balance

$$P_{\text{G}} - P_{\text{L}} - P_{\text{HP}} + P_{\text{PV}} + P_{\text{BESS}} = 0, \qquad (21)$$

where P_{G}, P_{L}, P_{HP}, P_{PV} and P_{BESS} are the grid, load, heat pump, PV and battery's electric power. In the case of the grid, a positive value means purchase, and for the battery, a positive value represents the discharge. The thermal network comprises a pipe system that transfers the thermal power from the solar collector $\dot{Q}_{\text{SC}}$, the thermal energy storage system $\dot{Q}_{\text{TESS}}$, and the heat pump $\dot{Q}_{\text{HP}}$ to the house, following the thermal power balance

$$\frac{\Delta T_{\text{in}}}{\Delta t} \sum_{i=1}^{n} m_i c_i = \dot{Q}_{\text{SC}} + \dot{Q}_{\text{TESS}} + \dot{Q}_{\text{HP}} - \dot{Q}_{\text{D}}. \qquad (22)$$

The parameters used for the simulations can be found in the source code of the model in [15].

III. GENETIC ALGORITHM

We used genetic algorithms to determine the power setpoint for each controllable element within a prediction horizon h. To obtain the setpoint profile for each device, we encoded the power setpoints as genes in a chromosome. A gene determines the setpoint value δ for each device at a particular instant in the future. Those genes are grouped per timestep; this way, there is a chromosome section that includes the setpoints of all the devices for each instant $(k+i|k)$ between $(k|k)$ and $(k+h|k)$, as shown in Fig. 1. In this work, we proposed calling those genes *setpoint genes*. Similarly, the last gene of the chromosome, which we defined as *suitability gene*, contains the overall performance of that control profile, which is used to build the Pareto front. To overcome possible dimensionality issues, we proposed a discrete-continuous approach for the setpoints, as, in reality, some devices work on an on/off basis. Such devices are the solar collectors, the TESS and the HP. In the case of the solar collectors, the power is sent by default to the house; if they are not activated and there is power available, it will be used to charge the TESS. On the other hand, the BESS is intrinsically continuous, and we considered power curtailment; therefore, the PV is also. To implement the curtailment at the gene level, we considered values from 0 to 1, where 1 is the maximum available PV power at the particular timestep. For the BESS, we proposed a set of functions of the SoC and

the BESS energy and power capacities to avoid unfeasible solutions to set the gene boundaries. Those functions are

$$\overline{P}_{\text{BESS}}^{\text{perm}}(k+i|k) = \begin{cases} P_{\text{BESS}}^{\text{max}} & \forall \quad P_{\text{BESS}} \geq P_{\text{BESS}}^{\text{max}} \\ C_{\text{BESS}}\Delta SoC_{\text{BESS}}^{\text{max}}(k+i|k) & \forall \quad P_{\text{BESS}} < P_{\text{BESS}}^{\text{max}} \end{cases}$$
(23)

and

$$\underline{P}_{\text{BESS}}^{\text{perm}}(k+i|k) = \begin{cases} C_{\text{BESS}}\Delta SoC_{\text{BESS}}^{\text{min}}(k+i|k) & \forall \quad P_{\text{BESS}} > -P_{\text{BESS}}^{\text{max}} \\ -P_{\text{BESS}}^{\text{max}} & \forall \quad P_{\text{BESS}} \leq -P_{\text{BESS}}^{\text{max}} \end{cases}$$
(24)

with

$$\Delta SoC_{\text{BESS}}^{\text{max}}(k+i|k) = \frac{SoC_{\text{BESS}}(k+i|k) - SoC_{\text{BESS}}^{\text{min}}}{\Delta t}$$
(25)

and

$$\Delta SoC_{\text{BESS}}^{\text{min}}(k+i|k) = \frac{SoC_{\text{BESS}}(k+i|k) - SoC_{\text{BESS}}^{\text{max}}}{\Delta t}.$$
(26)

This way, the only remaining constraint for the optimization problem is the TESS SoC. The thermal power from the TESS has to be 0 W if the temperature in the TESS is below the minimum allowed temperature (50 °C), and it cannot charge if its temperature is above the maximum allowed temperature (95 °C).

The optimization problem to solve with the GA comprises the multi-objective function

$$\min(C(k)) = \min(C_T(k), C_E(k), C_{\text{CO}_2}(k))$$
(27)

of the operational cost (OPEX)

$$C_E(k) = \sum_{k=0}^{h} \left(\sum_{i=1}^{n} P_i(k) c_i(k) + \sum_{i=1}^{n} \dot{Q}_i(k) c_i(k) \right) \Delta t,$$
(28)

the thermal comfort proposed by [21]

$$C_T(k) = \beta \sum_{k=0}^{h} \| T_{\text{set}}(k) - T_{\text{in}}(k) \|,$$
(29)

and the equivalent CO_2 emissions

$$C_{CO_2}(k) = \sum_{k=0}^{h} \left(\sum_{i=1}^{n} P_i(k) \, \text{CI}_i \right) \Delta t.$$
(30)

during the prediction horizon h. The best solution per objective will not necessarily be the best overall solution, i.e., the solutions are non-dominated. We used the Euclidean distance of the individual Pareto efficient solutions to the origin to select the best possible solution. This allowed us to obtain an overall cost per chromosome profile. The cost associated with the individual setpoint profile is then stored in the suitability gene, which is compared after the mating to determine the most suitable individual in the population, as shown in Fig. 1.

IV. RESULT ANALYSIS

We utilized the random forest regression approach as a proven short-term forecasting method [22]. This way, leveraging two years of historical data, we estimated the electric load demand, temperature (used to estimate the thermal demand), and irradiance (used to estimate the PV and solar collector

production). Our model specifically includes time lag, hour of the day, and month as features to effectively capture both immediate temporal dynamics and broader seasonal patterns. We partitioned the dataset into training and testing subsets, allocating 99 % for training to develop the model robustly and reserving 1 % for testing. The model, configured with 100 decision trees and a fixed random state of 42, ensures consistent and repeatable outcomes. A representative sample of the estimated values using a prediction of 60 min is presented in Fig. 2a and their respective error in Fig. 2b. These results highlight the model's precision, establishing its utility for our application.

We changed two parameters to evaluate the performance of the EMS: the season and the prediction horizon. For the former, we chose a representative week for winter and summer. For the latter, we determined a population size that ensures thermal comfort, as shown in Tables I and II. To feed the optimization, we used the dynamic prices shown in Fig. 3 and a carbon intensity of 0.325 gCO$_{2,\text{eq}}$/kWh. During winter (see Fig. 4), the EMS prioritizes the TESS over the HP as the latter would increase the electric load and energy cost (on 01/02). However, when the TESS SoC is lower, i.e., its temperature decreases, the thermal power it can deliver is reduced, and the EMS activates the HP to avoid uncomfortable temperatures (between 02/02 and 03/02). Finally, the HP becomes the dominant energy source once the TESS is discharged (between 04/02 and 07/02). The solar collectors provide some thermal power, but this is too small. During summer (see Fig. 5), the system again prefers the TESS to supply thermal power in the few cases where the indoor temperature falls below the setpoint temperature (between 19/07 and 22/07). Once the outdoor temperature is higher than the setpoint temperature, the TESS and the HP are not active, as the outdoor temperature would increase the indoor temperature, and no cooling technologies are considered (after 23/07).

TABLE I: Parameters used for the optimization in winter.

Horizon [min]	Population	Generations	Timestep run time [s]
0	25	5	0.3 - 0.55
30	50	5	0.3 - 0.65
60	100	5	0.44 - 0.85
90	200	5	0.7 - 1.2
120	400	5	0.7 - 1.65

TABLE II: Parameters used for the optimization in summer.

Horizon [min]	Population	Generations	Timestep run time [s]
0	25	5	0.3 - 0.7
30	200	5	0.4 - 1
60	750	5	1.3 - 2.2
90	1500	5	4 - 12
120	2000	5	5 - 9

From Fig. 4 and Table I, one can notice that the EMS performs more efficiently in winter. Even for the longer prediction horizon, a small population can solve the power
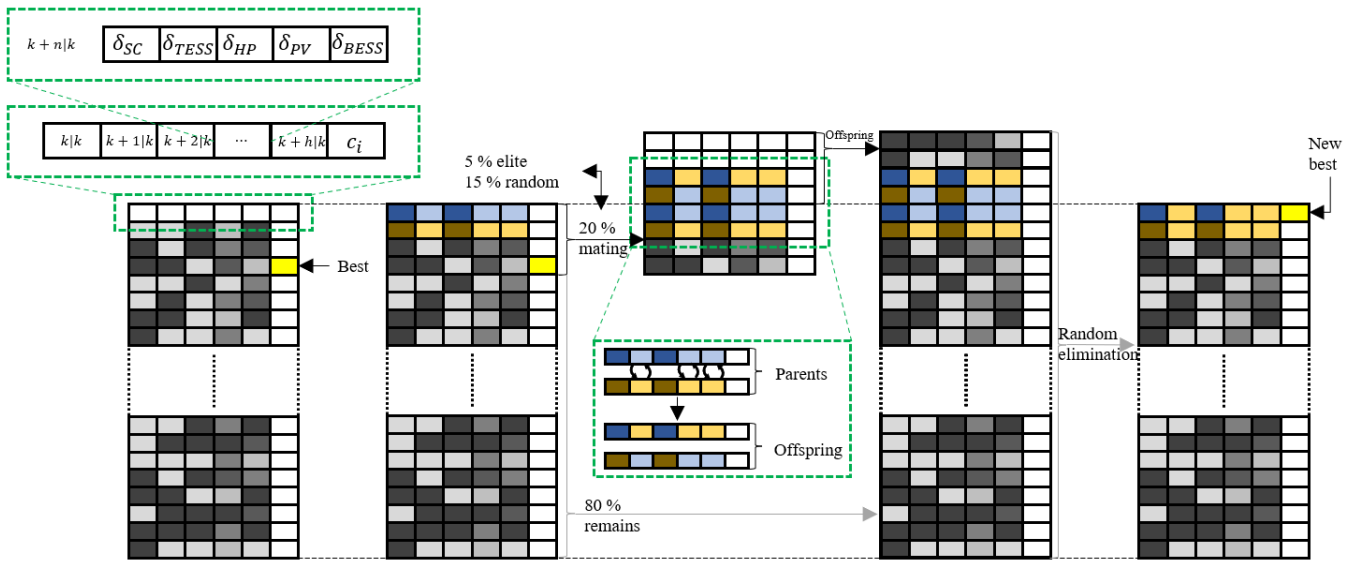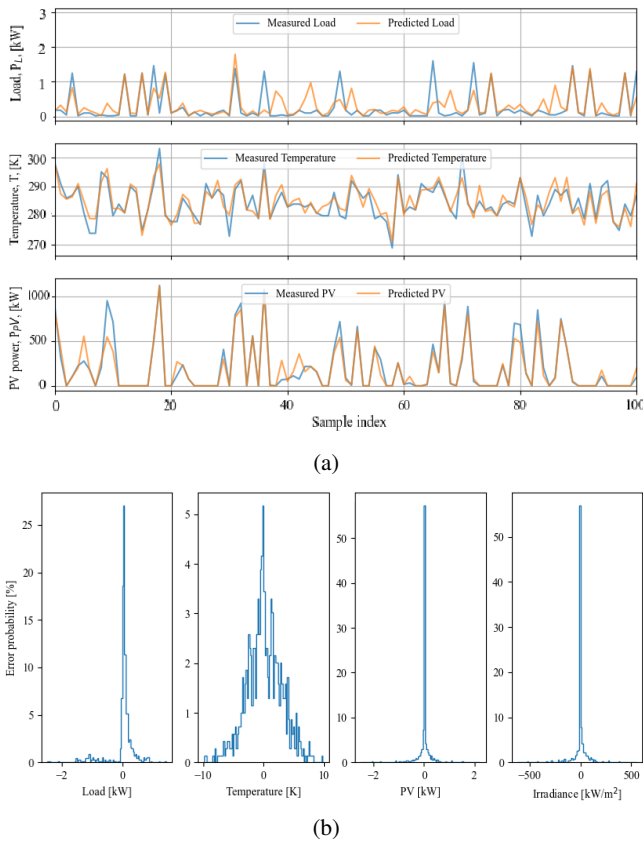
Fig. 1: Genetic Algorithm

(a)

(b)

Fig. 2: (a) Estimated and measured values and (b) error of the forecasted values using a prediction horizon of 60 min.

balance problem without increasing the indoor temperature. Similarly, having longer prediction horizons allows the EMS to keep the temperature closer to the setpoint when it reaches 20 °C. At night, when it lowers to 17 °C, the temperature drops naturally, and no thermal power is extracted from any source. Notice that the strategy can overcome the curse of dimensionality during winter, as achieving a control setpoint takes, on average, less than 1 s, albeit the cardinality of possible solutions when using a prediction horizon of 60 min is in the order of 10^{13}, as shown in Fig. 6b.

On the other hand, temperature control during summer is more challenging for the EMS in longer prediction horizons, as shown in Fig. 5 and Table II. Despite increasing the population one order of magnitude compared to the respective case in winter, the EMS during summer still executes heating instructions when the indoor temperature is above the setpoint (see Figs. 4c and 4d). This can be explained due to the absence of cooling mechanisms. During winter, the EMS can successfully prioritize the available thermal power sources, as explained before. In summer, however, as the outdoor temperature is already above the setpoint, any thermal action would increase the indoor temperature, decreasing thermal comfort and requiring all the setpoint genes to be zero for the thermal generation devices. For this reason, a more diverse gene pool is required to achieve the suboptimal solutions, increasing the time of simulation needed, as shown in Fig. 6. To overcome this challenge, one can take several action points aside from increasing the population or the number of generations. For example, the heating devices can be turned off at the gene level when the outdoor temperature reaches a specific value, or a hard constraint can be included as a condition to reach a solution during the evolutionary process.

The optimization performance per objective is shown in Tables III and IV for winter and summer, respectively. For both seasons, one can notice that the real-time control ($h = 0$
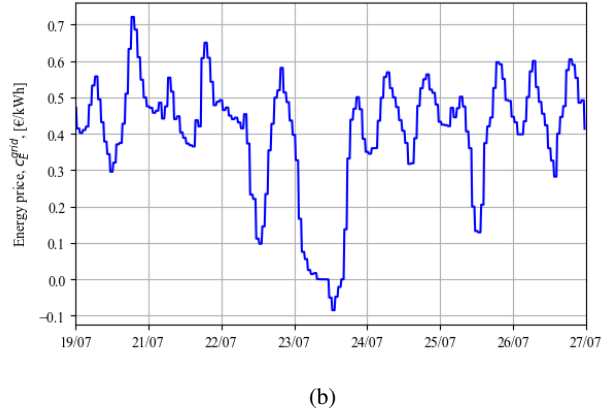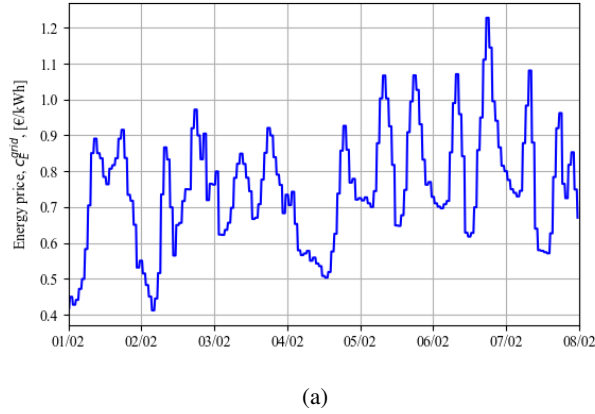
1041

Fig. 3: Energy price from the grid during (a) winter and (b) summer.

TABLE III: Optimization results in winter.

Horizon [min]	Grid purchase [kWh]	Grid cost [€]	Emissions [gCO$_{2,eq}$]	Thermal comfort [-]
0	67.28	13.80	21.87	3976
30	71.69	14.45	23.30	3891
60	72.81	14.62	23.66	3911
90	73.06	14.72	23.74	3926
120	73.35	14.84	23.84	3943

TABLE IV: Optimization results in summer.

Horizon [min]	Grid purchase [kWh]	Grid cost [€]	Emissions [gCO$_{2,eq}$]	Thermal comfort [-]
0	44.17	4.52	14.36	4584
30	46.38	4.71	15.08	4691
60	49.00	5.07	15.93	4650
90	49.23	5.18	16.00	4657
120	50.15	4.92	16.30	5679

min) has the best performance. This can be associated with the forecast, as the real-time control case does not depend on the prediction value and, therefore, does not have to account for the uncertainty. In contrast, the cases with longer horizons tend to have the lowest performances. Nevertheless, it is interesting to notice that, although the performance decreases when increasing the horizon, the change is relatively small between consecutive cases (less than 1 % for winter and 5 % for summer).

V. CONCLUSIONS

The results suggest that the forecast method and the energy management system perform satisfactorily. Thanks to its design, the EMS is easily adaptable to any MCES architecture, as the devices are added as genes. Energy storage systems' physical constraints are set at the gene level using the approach demonstrated for BESS, based on their allowed power, capacity, and SoC, minimizing unfeasibilities. Also, considering the devices that work on an on/off pace, such as the heat pump or the solar collectors, as binary at the gene level demonstrates

that the discrete-continuous approach for the power setpoints reduces the dimensionality issues. The random forest regression produced short-term estimations of the electric load, the temperature, and the irradiance with error distributions centred near 0 %, allowing us to estimate the thermal demand and PV output. With those estimations, the energy management system created a power setpoint profile for each device of the multi-carrier energy system, minimizing the economic cost, CO$_{2,eq}$ and ensuring thermal comfort. The low computational cost of the EMS proposed was also demonstrated for short-term prediction horizons. During winter, the EMS can solve the power allocation problem, including the prediction, in around 1 s on average for prediction horizons equal to or shorter than 120 min. In summer, the decisions might take up to 10 s per timestep, which is still acceptable, as the system works on a 15-minute timestep. Further research should be done to improve the performance of the algorithm during the summer and study longer prediction horizons.

REFERENCES

[1] J. Alpízar-Castillo, L. Ramirez-Elizondo, and P. Bauer, "Assessing the role of energy storage in multiple energy carriers toward providing ancillary services: A review," *Energies*, vol. 16, no. 1, 2023. [Online]. Available: https://www.mdpi.com/1996-1073/16/1/379

[2] J. Alpízar-Castillo, L. Ramírez-Elizondo, and P. Bauer, "The effect of non-coordinated heating electrification alternatives on a low-voltage distribution network with high pv penetration," in *2023 IEEE 17th International Conference on Compatibility, Power Electronics and Power Engineering (CPE-POWERENG)*, 2023, pp. 1–6. [Online]. Available: https://ieeexplore.ieee.org/document/10227394

[3] A. R. Abbasi and D. Baleanu, "Recent developments of energy management strategies in microgrids: An updated and comprehensive review and classification," *Energy Conversion and Management*, vol. 297, p. 117723, 2023. [Online]. Available: https://www.sciencedirect.com/science/article/pii/S0196890423010695

[4] P. Horrillo-Quintero, P. García-Triviño, E. Hosseini, C. A. García-Vázquez, H. Sánchez-Sainz, C. E. Ugalde-Loo, V. Peric, and L. M. Fernández-Ramírez, "Control of electrical/thermal multi-energy micro-grid," in *2023 IEEE International Conference on Energy Technologies for Future Grids (ETFG)*, 2023, pp. 1–6.

[5] M. Kazemi, C. Papadimitriou, N. G. Paterakis, I. Dukovska, and K. Kok, "Optimal design of multi-carrier and multi-objective home energy management system," in *2023 International Conference on Smart Energy Systems and Technologies (SEST)*, 2023, pp. 1–6.
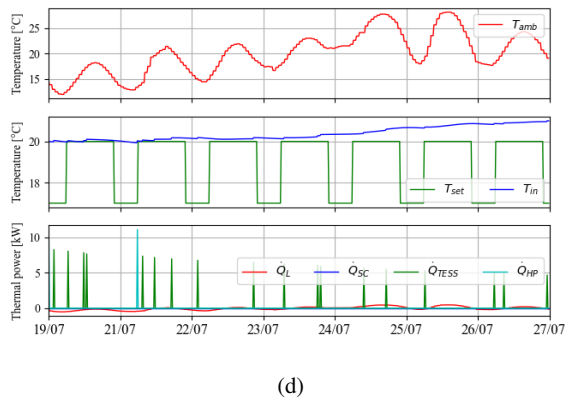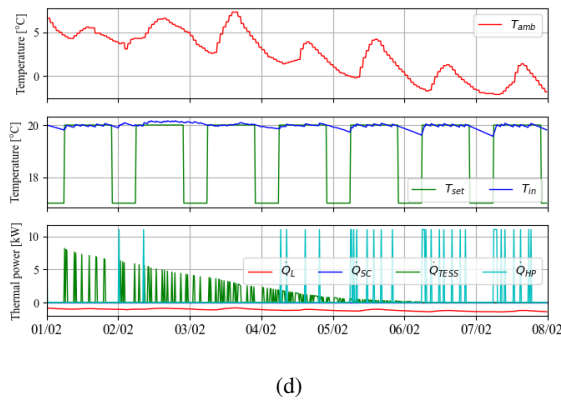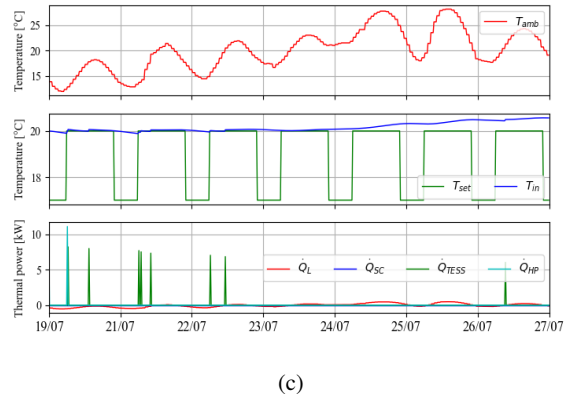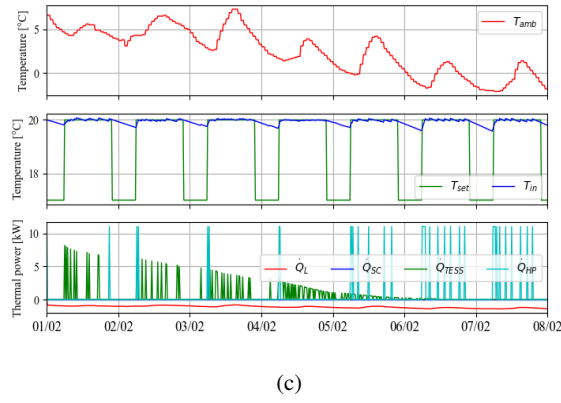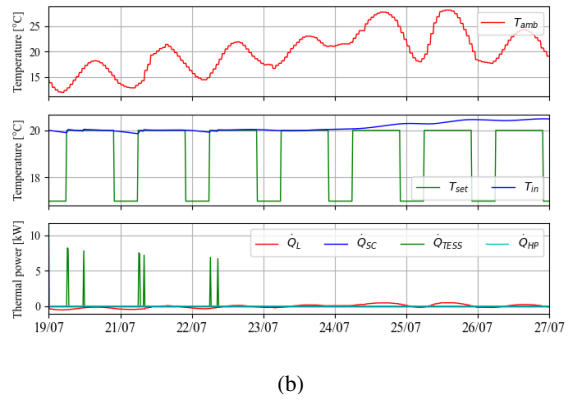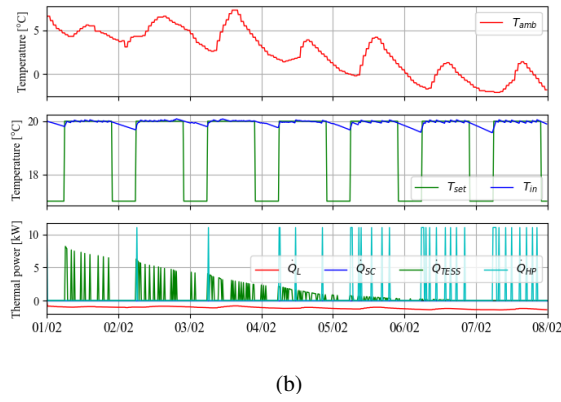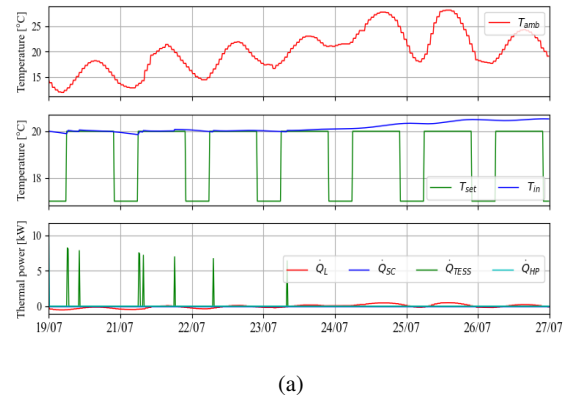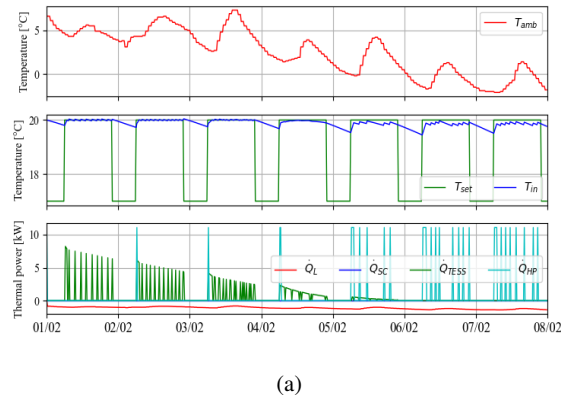
Fig. 4: Thermal power allocation during winter for prediction horizons of (a) 0, (b) 60, (a) 90, and (b) 120 min.

Fig. 5: Thermal power allocation during summer for prediction horizons of (a) 0, (b) 60, (a) 90, and (b) 120 min.

1043

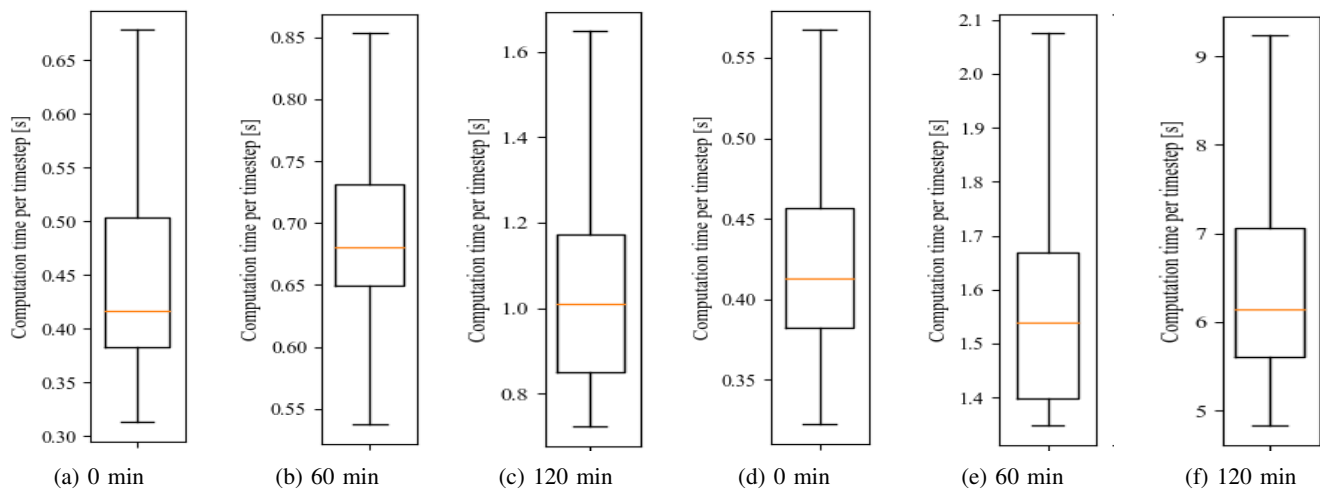| (a) 0 min | (b) 60 min | (c) 120 min | (d) 0 min | (e) 60 min | (f) 120 min |

Fig. 6: Distribution of the computational time required to solve each control iteration for different prediction horizons during winter (a), (b) and (c), and summer (d), (e) and (f). The model was run in a laptop with a processor Intel i7-1185G7, and 16 GB of RAM.

[6] P. Di, Z. Su, Q. Lu, J. Liu, K. Xu, and G. Yan, "Optimal energy management for multi-energy microgrid considering demand response," in *2022 IEEE 6th Conference on Energy Internet and Energy System Integration (EI2)*, 2022, pp. 72–77.

[7] Y. Li, H. Zhang, X. Liang, and B. Huang, "Event-triggered-based distributed cooperative energy management for multienergy systems," *IEEE Transactions on Industrial Informatics*, vol. 15, no. 4, pp. 2008–2022, 2019.

[8] D. Slaifstein, J. Alpízar-Castillo, A. M. Agudin, L. Ramírez-Elizondo, G. R. C. Mouli, and P. Bauer, "Aging-aware battery operation for multicarrier energy systems," in *IECON 2023- 49th Annual Conference of the IEEE Industrial Electronics Society*, 2023, pp. 1–8. [Online]. Available: https://ieeexplore.ieee.org/document/10312455

[9] X. Zhou, Z. Ma, S. Zou, J. Zhang, and Y. Guo, "Distributed energy management of double-side multienergy systems via sub-gradient averaging consensus," *IEEE Transactions on Smart Grid*, vol. 14, no. 2, pp. 979–995, 2023.

[10] T. M. Alabi, E. I. Aghimien, F. D. Agbajor, Z. Yang, L. Lu, A. R. Adeoye, and B. Gopaluni, "A review on the integrated optimization techniques and machine learning approaches for modeling, prediction, and decision making on integrated energy systems," *Renewable Energy*, vol. 194, pp. 822–849, 2022. [Online]. Available: https://www.sciencedirect.com/science/article/pii/S0960148122007741

[11] D. Arnone, M. Bertoncini, G. Paternò, A. Rossi, M. G. Ippolito, and E. R. Sanseverino, "Smart multi-carrier energy system: Optimised energy management and investment analysis," in *2016 IEEE International Energy Conference (ENERGYCON)*, 2016, pp. 1–6.

[12] P. Horrillo-Quintero, P. García-Triviño, E. Hosseini, C. Andrés García-Vázquez, H. Sánchez-Sainz, C. E. Ugalde-Loo, V. S. Perić, and L. M. Fernández-Ramírez, "Dynamic fuzzy logic energy management system for a multi-energy microgrid," *IEEE Access*, vol. 12, pp. 93 221–93 234, 2024.

[13] H. Xiao, X. Pu, W. Pei, L. Ma, and T. Ma, "A novel energy management method for networked multi-energy microgrids based on improved dqn," *IEEE Transactions on Smart Grid*, vol. 14, no. 6, pp. 4912–4926, 2023.

[14] D. Song, W. Meng, M. Dong, J. Yang, J. Wang, X. Chen, and L. Huang, "A critical survey of integrated energy system: Summaries, methodologies and analysis," *Energy Conversion and Management*, vol. 266, p. 115863, 2022. [Online]. Available: https://www.sciencedirect.com/science/article/pii/S0196890422006598

[15] J. Alpízar-Castillo, "GA HEMS," https://github.com/jjac13/GA_HEMS, 2023.

[16] J. Alpízar-Castillo, V. Vega-Garita, N. Narayan, and L. Ramirez-Elizondo, "Open-access model of a PV-BESS system: Quantifying power and energy exchange for peak-shaving and self consumption applications," *Energies*, vol. 16, no. 14, 2023. [Online]. Available: https://www.mdpi.com/1996-1073/16/14/5480

[17] N. Damianakis, G. C. R. Mouli, and P. Bauer, "Risk-averse estimation of electric heat pump power consumption," in *2023 IEEE 17th International Conference on Compatibility, Power Electronics and Power Engineering (CPE-POWERENG)*, 2023, pp. 1–6.

[18] J. Alpízar-Castillo, L. M. Ramírez-Elizondo, and P. Bauer, "Modelling and evaluating different multi-carrier energy system configurations for a dutch house," *Applied Energy*, vol. 364, p. 123197, 2024. [Online]. Available: https://www.sciencedirect.com/science/article/pii/S0306261924005804

[19] M. Pipattanasomporn, M. Kuzlu, S. Rahman, and Y. Teklu, "Load profiles of selected major household appliances and their demand response opportunities," *IEEE Transactions on Smart Grid*, vol. 5, no. 2, pp. 742–750, 2014.

[20] R. American Society of Heating and I. A. Air-Conditioning Engineers, *2021 ASHRAE® Handbook - Fundamentals (SI Edition)*. American Society of Heating, Refrigerating and Air-Conditioning Engineers, Inc. (ASHRAE), 2021.

[21] A. Baniasadi, D. Habibi, O. Bass, and M. A. S. Masoum, "Optimal real-time residential thermal energy management for peak-load shifting with experimental verification," *IEEE Transactions on Smart Grid*, vol. 10, no. 5, pp. 5587–5599, 2019.

[22] L. Gigoni, A. Betti, E. Crisostomi, A. Franco, M. Tucci, F. Bizzarri, and D. Mucci, "Day-ahead hourly forecasting of power generation from photovoltaic plants," *IEEE Transactions on Sustainable Energy*, vol. 9, no. 2, pp. 831–842, 2018.